Amorphous and nanocrystalline luminescent Si and Ge obtained via a solid-state chemical metathesis synthesis route

Paul F. McMillan[a,b,*], Jan Gryko[c], Craig Bull[d], Richard Arledge[c], Anthony J. Kenyon[e], Barbara A. Cressey[f]

[a]Christopher Ingold Laboratory, Materials Chemistry Centre, Department of Chemistry, University College London, 20 Gordon Street, London WC1H 0AJ, UK
[b]Davy Faraday Research Laboratory, Royal Institution of Great Britain, London W1S 4BS, UK
[c]Department of Physical and Earth Sciences, Jacksonville State University, AL 36265, USA
[d]School of Physics and Centre for Science at Extreme Conditions, University of Edinburgh, Mayfield Road, Edinburgh EH9 3JZ, UK
[e]Department of Electronic and Electrical Engineering, University College London, Torrington Place, London WC1E 7JE, UK
[f]Science and Engineering Electron Microscopy Centre, School of Chemistry, University of Southampton, Highfield, Southampton SO17 1BJ, UK

Abstract

A new solid-state metathesis synthesis route was applied to obtain bulk samples of amorphous or microcrystalline Si and Ge. The method involves reaction of Zintl phases such as NaSi or NaGe, with ammonium or metal (e.g., CuCl, CoBr$_2$) halides. The driving force for the solid-state reaction is provided by the formation of alkali halides and the transition metals or metal silicides, or gaseous ammonia and hydrogen. The semiconductors were purified by washing to remove other solid products. The amorphous semiconductors were obtained in bulk form from reactions carried out at 200–300 °C. Syntheses at higher temperatures gave rise to microcrystalline semiconductors, or to micro-/nanocrystalline particles contained within the amorphous material. Similar crystalline/amorphous composites were obtained after heat treatment of bulk amorphous materials.
© 2005 Elsevier Inc. All rights reserved.

1. Introduction

Silicon and germanium are important semiconducting materials that are used in bulk or thin film form as both crystalline and amorphous solids. The amorphous forms have been developed particularly for use in photovoltaic devices [1]. Nanocrystalline particles of the group IV elements, either free-standing or incorporated in solid matrices, are now under development because of their useful photo- and electro-luminescent properties [2–7]. Here we report a solid-state chemical synthesis route that can be used to obtain bulk samples of amorphous or microcrystalline silicon and germanium materials, that can also yield luminescent nanoparticles embedded within an amorphous solid matrix.

The synthesis method involves reacting polyanionic "Zintl phases" (e.g., NaSi, NaGe) together with metal halides (e.g., CuCl, CoBr$_2$) or ammonium salts (NH$_4$Cl, NH$_4$Br). Sodium silicide is an ionic Zintl phase that contains isolated Si$_4^{4-}$ tetrahedral clusters surrounded by Na$^+$ ions [8] (Fig. 1). The formation reaction proceeds via a chemical "metathesis" process, in which ionic salts (alkali halides) are formed as products, together with solid metals (Cu, Co) or gaseous NH$_3$, as well as the elemental semiconductors (Si, Ge); e.g.,

$$CuBr(s) + NaSi(s) = NaBr(s) + Si(s) + Cu(s). \quad (1)$$
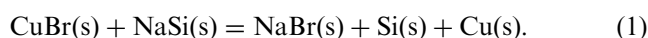
Depending upon the transition metal used, metal silicides (e.g., FeSi$_2$) are also occasionally formed in the

---

*Corresponding author. Christopher Ingold Laboratory, Materials Chemistry Centre, Department of Chemistry, University College London, 20 Gordon Street, London WC1H 0AJ, UK. Fax: +44 207 679 7463.
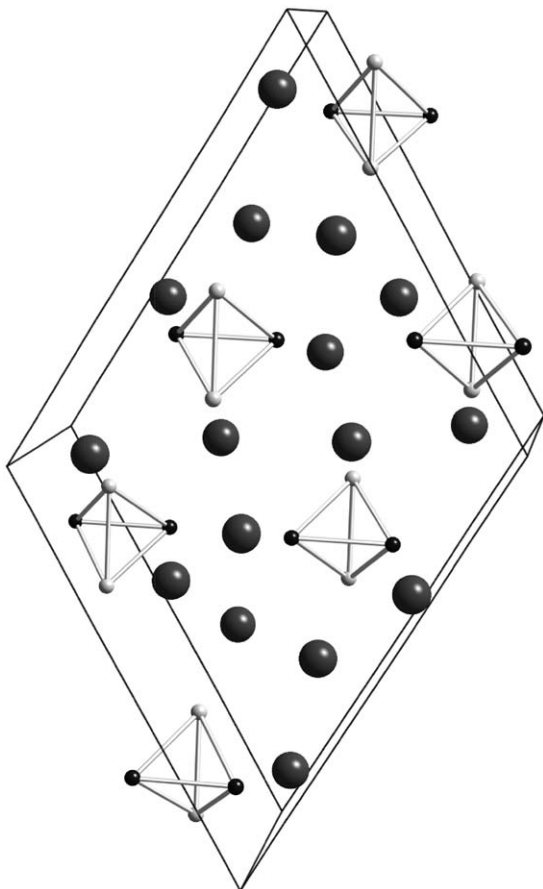
E-mail address: p.f.mcmillan@ucl.ac.uk (P.F. McMillan).

Fig. 1. The monoclinic Zintl phases NaSi and NaGe contain isolated Si_4^{4-} or Ge_4^{4-} tetrahedral groupings, as in the isoelectronic and isostructural elemental allotrope of white P, surrounded by alkali cations (shown as gray balls). The compounds are highly reactive to atmospheric oxidation and hydration reactions, because of the exposed Na^+ species, and also due to the exposed electron lone pairs on the pyramidal 3-coordinated Si atoms, and they must be handled in strictly controlled low O_2/H_2O environments via glove box or Schlenck line techniques. They are thus also ideal chemical precursors for metastable/metathesis synthesis routes, that require products with a high value of the chemical potential, compared with the desired products.

synthesis reaction. To purify the elemental semiconductors formed by reaction (1), other solid products are readily removed by washing in water, dilute acid, or methanol/ethanol. In order to minimize or avoid the washing steps, we also investigated the use of ammonium bromide or chloride as reagents in the related metathesis reactions; e.g.,

$$NH_4Br(s) + NaSi(s)$$
$$= NaBr(s) + Si(s) + NH_3(g) + 1/2H_2(g). \qquad (2)$$
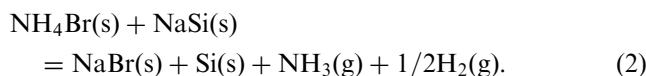
In this case, NH_3 and H_2 gases are expelled from the system during synthesis, and the amorphous semiconductor is recovered (in nominally pure form) after

minimal washing in water to remove the alkali halide. We found that the physical state of the semiconductor produced (i.e., amorphous vs. crystalline material, as determined by X-ray powder diffraction) depends both upon the precursors used, and the reaction temperature. Analogous metathesis reactions provide a general approach to solid-state synthesis, that has been applied to a wide range of materials including various nitrides, tetrelides, and chalcogenide compounds [9,10]. Related reactions using Zintl phase precursors have also recently been used to give rise to Si- and Ge-containing luminescent nanoparticles in organic liquid suspension [11,12].

2. Experimental methods

All solid-state Zintl phase precursors were prepared and handled using glove box techniques (<10 ppm O_2/H_2O). Metathesis reactions were carried out inside sealed SiO_2 glass tubes, with samples contained within Ta crucibles or wrapped in Ta/Mo foil. The synthesis reactions were carried out at 200–500 °C, for periods ranging between 10 and 20 h. The solid products were then washed in water, dilute acid (e.g., HNO_3) and/or ethanol/methanol, to remove various alkali halides and transition metals or metal silicides that were produced in the reactions.

The products were initially characterized by powder X-ray diffraction (Siemens D-5000: $CuK\alpha$ radiation), and by Raman spectroscopy (514.5 nm excitation), using a home-built high-throughput spectrograph based on Kaiser super-notch filters and a CCD detector [13]. Photoluminescence data were obtained with Ar^+ (476 nm) laser excitation using a Bentham M300 single-grating monochromator and photomultiplier detection system [4]. PL spectra were corrected for the optical response of the system, and temperature effects due to heating by the incident laser (300–400 °C) were determined by a Planck fit to the corrected intensity data between 1000 and 1700 nm. Initial FTIR spectra were obtained by powder transmission on samples pressed into KBr discs: later samples were examined by transmission/reflectance spectroscopy of pure materials, that were either pressed into plates between diamonds in a diamond anvil cell, or as free-standing powdered samples, using a Bruker IFSv-66 microbeam FTIR system.

Solid-state ^{29}Si MAS-NMR spectra were obtained using a Bruker MSL-300 (7 T), corresponding to a Larmor frequency $\omega_L = 59.60$ MHz for ^{29}Si; chemical shifts were referenced to TMS ($(CH_3)_4Si$). Samples were spun at 5.5 kHz, using a 30° pulse with a 2 min recycle time. ^1H–^{29}Si cross-polarized (CP) spectra were obtained using a decoupling field of 50 kHz and 10 ms contact time. Selected samples were also run using

analogous single-pulse and ^{1}H–^{29}Si CP conditions using a Varian-Unity spectrometer operating at 9.4 T ($\omega_L = 79.46$ MHz for ^{29}Si).

Samples were examined by scanning electron microscopy (SEM), and chemical compositions were obtained via energy dispersive analysis, using either the SEM or a JEOL 8600 electron microprobe. Selected samples were also studied by transmission electron microscopy (TEM) via imaging and selected area diffraction techniques, using a JEOL JEM 2000-FX instrument operating at 200 kV (Southampton). Samples were prepared by standard techniques as grain dispersions supported on carbon films on Cu TEM specimen holders.

3. Results and discussion

3.1. Products formed and X-ray diffraction studies

The amorphous/crystalline semiconductor products were prepared by reactions (1) or (2) at $T = 200-500\,°C$, using NaSi/NaGe as precursors, mixed with various transition metal (Cu, Fe, Mn) or ammonium halides (Cl, Br). Using metal halide precursors, reactions were driven by exothermic formation of alkali halides and the solid elements. Mixtures treated at $T > 300\,°C$ resulted in formation of microcrystalline Si/Ge samples, along with metal particles mixed with the alkali halides according to reaction (1). In a few cases, transition metal silicides (e.g., $FeSi_2$, $CoSi_2$) were also formed in the reaction. After completion of the metathesis reactions, the various solid halides, silicides and metal particles were removed from the samples by washing with H_2O, dilute acid (HNO_3), and/or alcohol (ethanol/methanol).

During syntheses carried out at lower T (200–300 °C), it was generally observed that no crystalline semiconductors, but only amorphous Si or Ge, were obtained, as revealed by X-ray diffraction and Raman scattering (Fig. 2). The bandgap of a sample of a-Si synthesized via reaction (1) was determined to be 1.129 eV via electrical
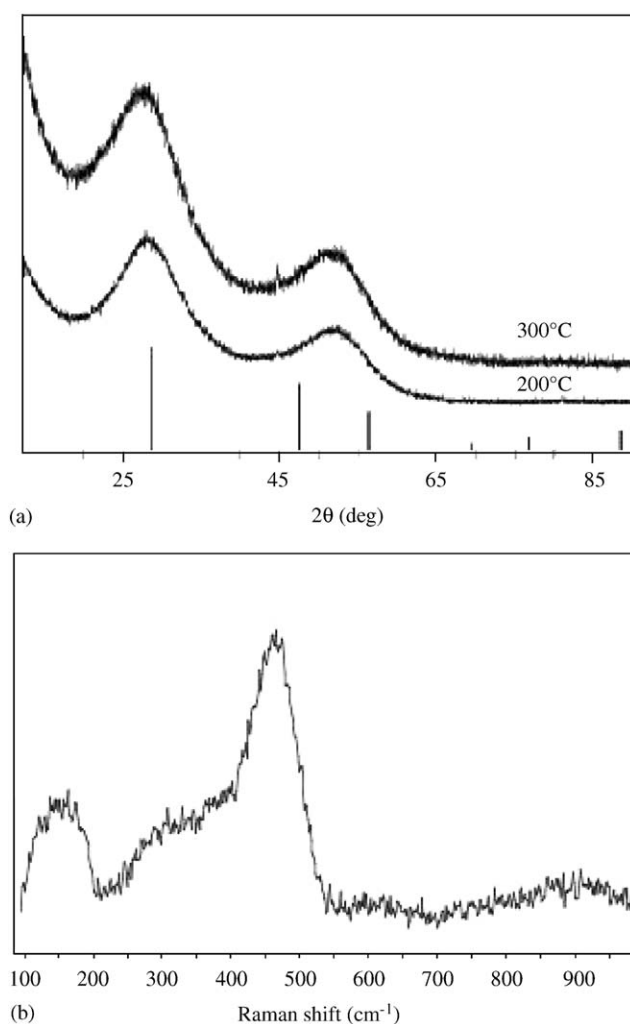
Fig. 2. (a) X-ray diffraction patterns of amorphous silicon samples synthesized by reaction between metal halides or NH_4Cl and NaSi at 200 and 300 °C, after washing to remove the other solid products. The lines below the amorphous diffraction pattern indicate the positions and intensities of the powder diffraction lines for crystalline Si. (b) Raman scattering of a-Si synthesized via reaction (2) between NH_4Cl and NaSi at 200 °C. The features above 550 cm^{-1} are due to multiphonon scattering.
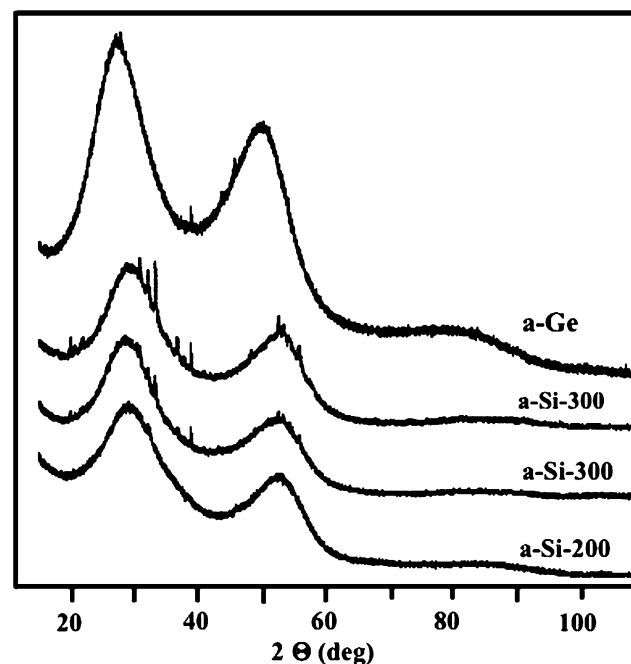
Fig. 3. X-ray diffraction patterns of a-Si and a-Ge samples synthesized by metathesis reactions (1) or (2), after washing to remove other solid products. Weak crystalline features are sometimes apparent in the spectra, as observed for the "a-Si-300" samples, dependent upon the batch, especially for higher temperature syntheses. These additional diffraction peaks can be assigned to the semiconductor clathrate phase Na_8Si_{46}, that is usually obtained by controlled thermal decomposition of the Zintl phase NaSi.

conductivity measurements on pressed discs of powdered material.

In syntheses carried out via reaction (2), the (Si/Ge) semiconductor products obtained generally remained amorphous to X-ray diffraction, to higher reaction temperatures than those formed by reaction (1). This is explained by the formation of volatile products (NH_3, H_2), that carry away part of the reaction enthalpy [10]. For reactions carried out at $T > 300\,°C$, weak additional crystalline peaks occasionally appeared in X-ray diffraction patterns (Fig. 3). These peaks are identified as due to "semiconductor clathrate" phases, e.g., Na_8Si_{46} [14–16], that are formed metastably during the synthesis process. These low-density clathrate materials are usually made by controlled thermal decomposition of the Zintl phase precursor (e.g., NaSi, NaGe). The metathesis reactions could thus provide a new route to the semiconducting (or semimetallic) clathrate-structured phases.

During X-ray characterization of the amorphous semiconductors produced by reactions (1) and (2),

subtle differences were noted in the position, width and relative amplitude of the "first sharp diffraction peak" (FSDP) between different synthesis runs (Figs. 2 and 3). It is known that the position and appearance of the FSDP scales with the density among amorphous materials [17]. The density of amorphous silicon samples prepared by e^--beam deposition on crystalline Si, or by ion bombardment of c-Si, has been determined to range between 2.26 and $2.29\,g/cm^3$, approximately 1.8–3.0% less dense than the crystalline semiconductor ($2.33\,g/cm^3$) [18]. Our bulk samples prepared by chemical synthesis exhibited an average density slightly lower than this range of values, approximately 2.0–$2.1\,g/cm^3$, as determined by sink-float techniques.

We also observed that most of the samples contained fractions with a significant "tail" to lower densities, down to $< 1.75\,g/cm^3$. During our studies, we separated some of the samples into density fractions for certain physical and spectroscopic investigations, because of the possibility of "polyamorphism" occurring within the
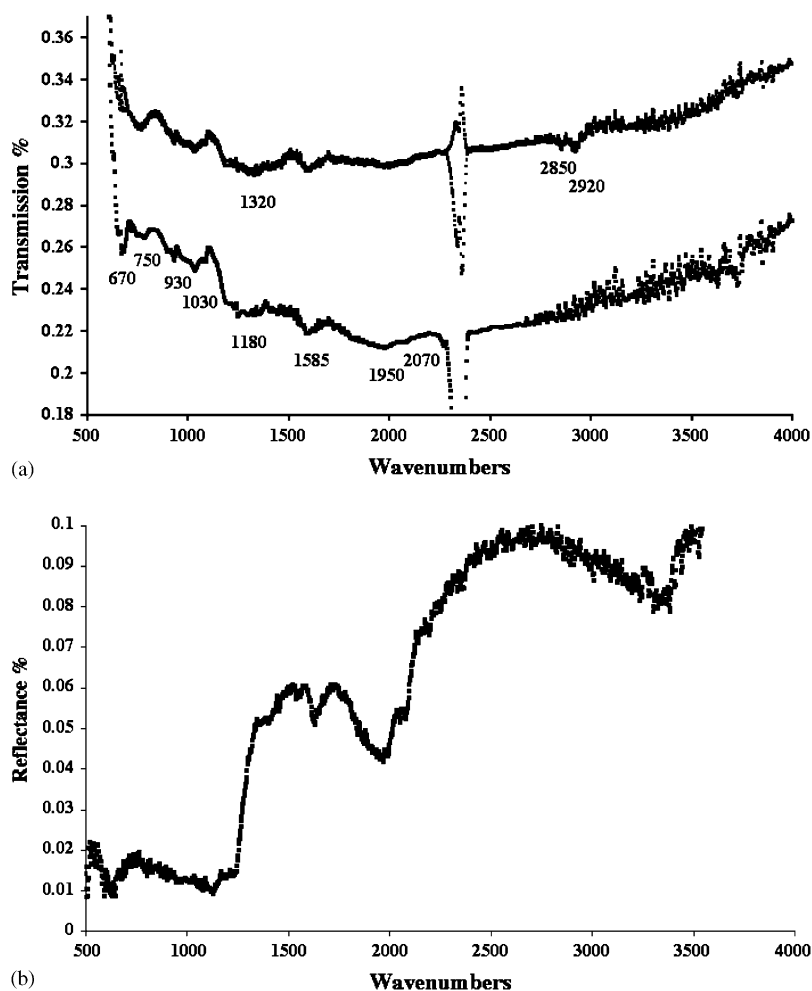

Fig. 4. (a) FTIR transmission and (b) reflectance transmittance spectra of an a-Si samples prepared via reaction (2), that did not contain any significant impurities such as oxygen. The reflectance spectrum is referenced to Au, that exhibits 100% reflectance across the IR range.

amorphous silicon, between a "normal" low-density a-Si (LDA), and a "very low-density" form (VLDA).

The concept of density-driven "polyamorphism", related to phase transitions occurring in simple liquids at constant composition, has been described among amorphous semiconductors, including Si and Ge, for many years [19–22]. It is now gaining wide acceptance, based on new experimental observations and results of MD simulations [23–27]. A low–high density amorphous transition (LDA–HDA) is present under high-pressure conditions, or during cooling from the metallic liquid. In the present work, we initially thought that a further polyamorphic transition could occur, between LDA and VLDA polyamorphs, accessed metastably during the solid-state metathesis synthesis. This was based on a consideration of metastable phase relationships occurring under "negative pressure" conditions [28,29]. However, after a suite of characterization studies on density-separated fractions of a-Si obtained

from various batches synthesized via reactions (1) and (2), we concluded that the differences observed within and between batches were most likely due to (a) partial crystallization of the samples (to give Si clathrates or nanocrystalline Si), or (b) to the presence of chemical impurities (H, and also O, N), included within the samples. However, the possibility of an LDA-VLDA polyamorphic transformation is still not excluded, just as in amorphous solid H_2O, there is now evidence for an additional very-high density (VHDA) form of amorphous ice [30,31], supplementing the already known HDA and LDA polyamorphs [32,33].

3.2. Chemical characterization of the samples

Apart from H, the primary chemical impurity detected within the samples was O, that was often found to be present in concentrations up to 3–5% by weight among earlier samples, but was reduced
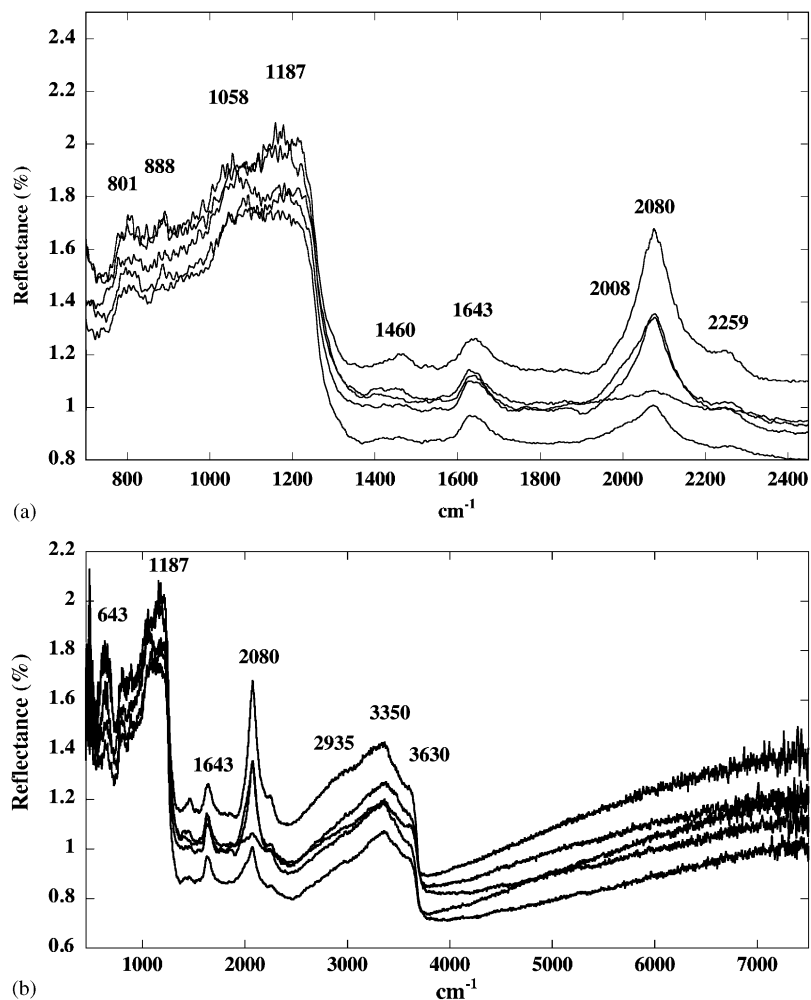

Fig. 5. FTIR spectrum taken in reflectance mode of pressed discs of an early batch of a-Si sample containing substantial amounts of O (10–15 at%), H (10 at%) and N (~8 at%) impurities, as determined for the bulk sample via chemical analysis. The spectra refer to different density fractions separated from a single sample. Because Si–H stretching and other features appear as positive peaks in the spectra, these features are likely due to a combination of reflectance and transmission effects at the sample surface. (a) Spectra from 700 to 2500 cm^{-1} showing the detail of Si–H and Si–O(N) stretching modes. (b) Full spectra between 430 and 7500 cm^{-1}.

to <1% in later synthesis batches. Because all samples were handled and reactions carried out in O-free environments, the oxidation reactions most likely took place during washing, or while samples from earlier batches were stored in air for up to several months.

Some of the earlier-synthesized batches were in fact found to contain very high oxygen contents, up to 10–20% by weight; they thus corresponded to amorphous SiO_x ($x \sim 1$) or to physical mixtures of a-Si/a-SiO_2. The oxide components gave rise to obvious features in the ^{29}Si NMR and also the FTIR spectra, described below. Some nitrogen was also be detected in some samples prepared by reaction (2), that we believe is likely to be incorporated in the amorphous matrix. The incorporation of O (or N) atoms into an amorphous Si matrix to form "siloxene" materials is thought to provide enhancement of the luminescence characteristics [2,34]; also the presence of amorphous/nanocrystalline Si, Ge particles in an O-, N-rich matrix is known to provide useful enhancement of the luminescence efficiency [4,6,34,35]. These points are discussed below. They are raised here to note that the serendipitous incorporation of O,N impurities in the a-Si (and a-SiO_x) materials obtained by chemical synthesis (and subsequent storage in air) is not necessarily a "bad" outcome: if controlled, it could lead to a useful new class of optoelectronic materials.

Hydrogen is a well-known impurity within a-Si; it is important for passivation of broken bond defects, and thus optimizing the electronic/photovoltaic properties of the amorphous semiconductor. Initial batches of a-Si prepared in this study were originally thought to contain minimal amounts of H, mainly because no Si–H vibrations could be detected by initial FTIR or Raman scattering spectroscopy carried out on the sample. Samples were taken to the Institut Laue-Langevin (ILL) in Grenoble for examination of their low-energy excitations by inelastic neutron scattering experiments (spectrometer stations IN6 and D7) [36]. However, during the neutron measurements, it was found that all of the samples contained substantial H, with concentrations ranging between 5 and 12 at% [37]. Because no Si–H species had been observed by the preliminary FTIR measurements on these materials, it was initially thought that the hydrogen might be present as molecular H_2 groups contained within the a-Si network [38–41]; attempts were made to remove such H-bearing species by annealing under high-vacuum conditions at $T = 300-450\,^\circ C$ [41]. However, as was revealed by later characterization experiments, that process resulted in partial recrystallization of the samples, yielding nanocrystalline Si particles embedded within the amorphous matrix [42–46]. These crystalline nanoparticles were later detected by TEM and Raman scattering spectroscopy: those results are described below.
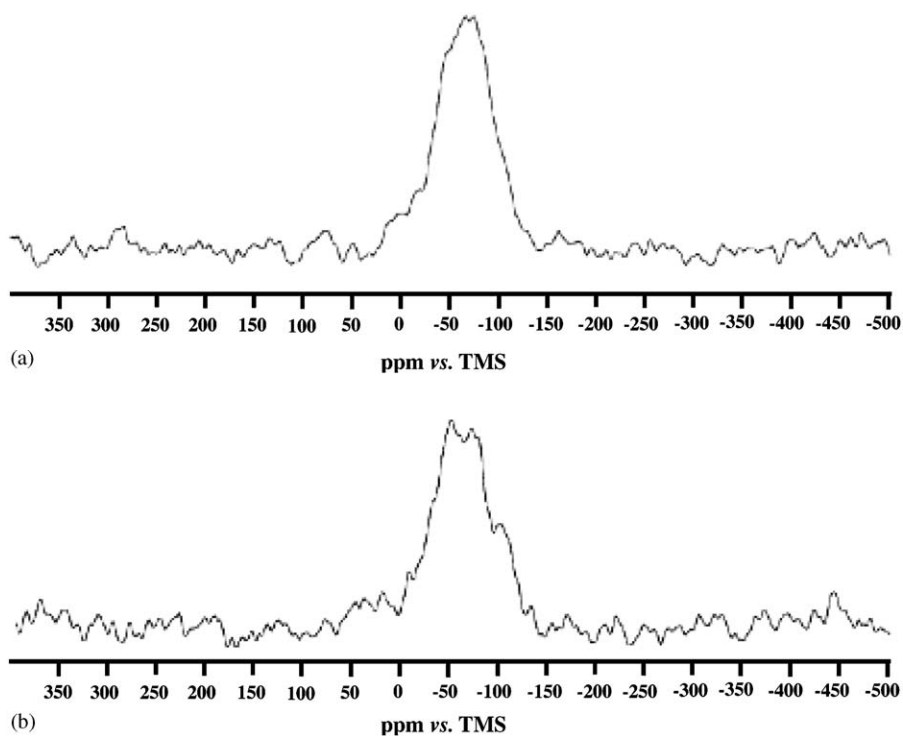

Fig. 6. (a) Single pulse ^{29}Si (30° pulse; 2 min recycle time, spun at 5.5 kHz) MAS NMR spectra of an a-Si sample containing no detectable impurities (O,N) by chemical analysis. (b) ^1H–^{29}Si CP spectrum of the same sample. The correspondence between the single pulse and ^1H-decoupled spectra indicates that the sample contains H impurities distributed randomly with respect to the Si sites.

3.3. FTIR spectroscopy

FTIR transmission and reflectance spectra were obtained from samples that were found to contain minimal O, N or H impurities (the H contents of samples prepared later in the study did not exceed approximately 2–5 at% H) (Fig. 4). Powdered materials were pressed into flat plates ∼10–50 μm thick between two diamonds in a diamond anvil cell, and then run in air (mounted on a KBr plate). Above the transmission cutoff due to phonon absorption (550–600 cm^{-1}), the transmission through the pressed discs was low, and only a few weak resonances were observed throughout the 500–4000 cm^{-1} region (Fig. 4(a)). (Fig. 4 contains a superposition of several transmission spectra: that is why the doublet near 2350 cm^{-1} due to atmospheric CO$_2$ appears as both positive and negative features in the plot.) Similar IR spectra were obtained for a-Si colloidal samples prepared by thermolysis of silanes in supercritical hexane [46].

The features associated with Si–H vibrations were best revealed in reflectance spectra, obtained from a single side of the same pressed disc samples (Fig. 4(b)). The reflectivity rises generally at higher energy values due to the impending band edge (1.129 eV = 9100 cm^{-1}). The dip in the reflectance spectrum at approximately 2000 cm^{-1} corresponds to Si–H vibrations in the sample. (The adjacent sharp dip at 1630 cm^{-1}, along with that near 3500 cm^{-1}, are due to H$_2$O adsorbed on the KBr disc used to support the sample.)

Some of the earlier batches of a-Si samples were found to contain substantial O (and N) impurities, as well as H. Later protocols that minimized uptake of O/H during washing and storage resulted in nearly pure a-Si and SiH$_x$ materials. FTIR reflectance spectra of density-separated fractions of an "impure" sample are shown in Fig. 5. These spectra clearly show features due to Si–H stretching and bending vibrations, and Si–O (and perhaps also Si–N) stretching [47–49]. The Si–H and Si–O features appear in the "reflectance" spectra as
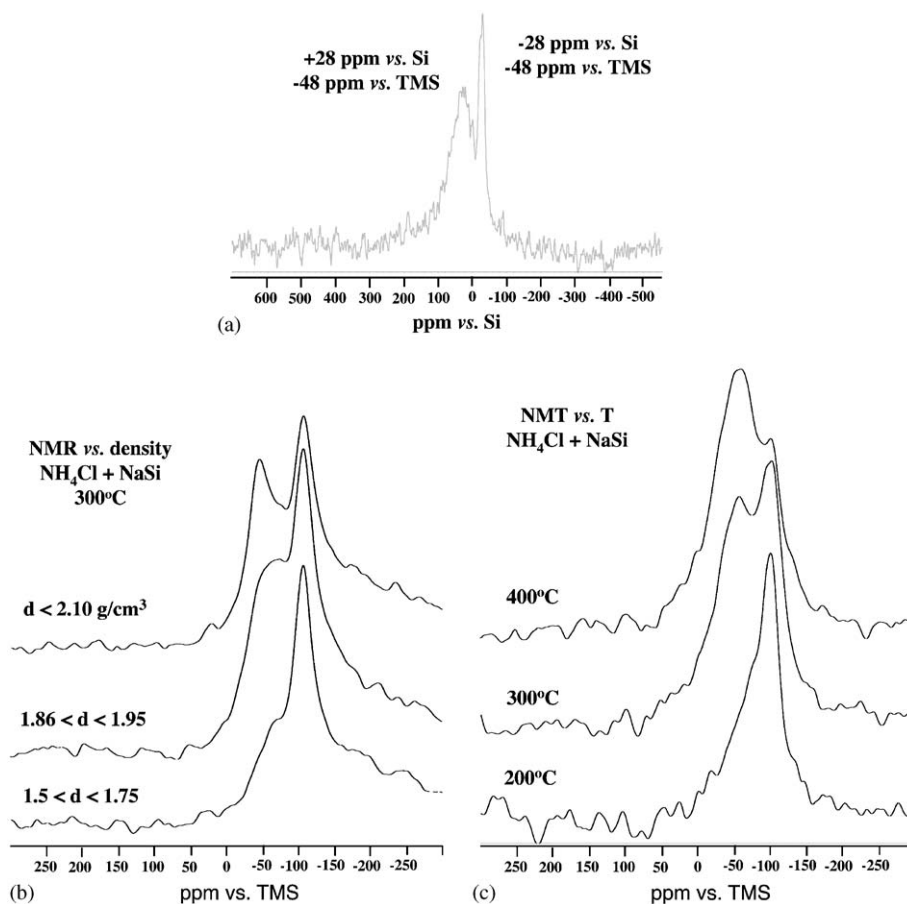

Fig. 7. (a) Single pulse ^{29}Si MAS NMR spectrum of a sample containing ∼10 at% O impurity. This spectrum (unlike the others presented here) is referenced to crystalline Si rather than TMS, so the peaks are shifted by 76.5 ppm relative to the chemical shift scale used for the other spectra. (b) single pulse ^{29}Si MAS NMR spectra of a-Si/SiO$_x$ samples prepared via reaction (2) (i.e., NaSi + NH$_4$Cl) at different temperatures (T = 200, 300, 400 °C). (c) ^{29}Si MAS NMR spectra of a-Si/SiO$_x$ materials within different density fractions separated from a sample prepared via reaction (2): bottom—1.50–1.75 g/cm^3; middle—1.86–1.95 g/cm^3; top—1.95–2.10 g/cm^3.

positive features that resemble the IR absorption spectra [46–49]. This could mean that they are due to absorption within thin films of impurity-rich material at the surface of the sample grains, or that their appearance in the reflectance spectrum is due to subtle effects on the optical constants, within a region of low reflectivity. We have already observed both positive and negative contributions to the IR reflectivity, from minor impurity resonances associated with O–H and C–O species in silicate glass samples [50,51]. The form of the reflectivity function in the infrared region is quite different to that recorded for a-Si samples that contained essentially no O and minor H impurities (Fig. 4). For the H, O(N)-containing samples (Fig. 5), broad absorption features at $\sim$630 cm^{-1} and in the 900–1000 cm^{-1} region are intrinsic to a-Si, and are due to combinations of transverse acoustic/optic phonons in the amorphous semiconductor [47–49]. In the Si–H stretching region, the envelope under the $\sim$2100 cm^{-1} band contains contributions from SiH, =SiH$_2$ and –SiH$_3$ mono- and polyhydride species, isolated or clustered within the bulk, and at surfaces [4,43,47–49]. From the integrated IR absorption band intensities in the Si–H stretching region, the bound H content is estimated to be between 5 and 15 at%, consistent with the neutron scattering experiments [36,37]. These samples that were determined to contain impurity O also exhibited features in the 1000–1100 cm^{-1} region and at $\sim$800 cm^{-1}, that are assigned to Si–O bond stretching and SiOSi linkages, respectively [4,34,46–48]. The samples also showed a
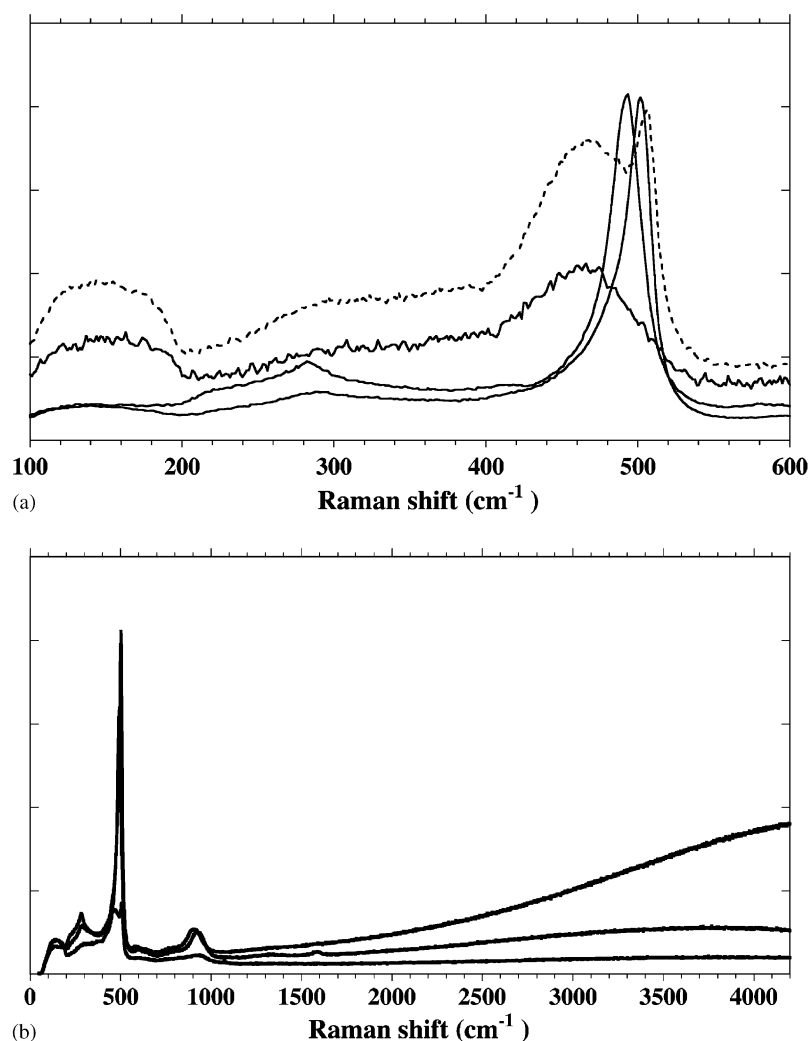

Fig. 8. (a) Raman spectra of various silicon samples prepared by metathesis synthesis. None of the materials exhibited crystalline peaks via X-ray diffraction. Most samples examined in the study were fully amorphous, and exhibited only a broad Si–Si stretching mode at $\sim$450 cm^{-1}. Other samples contained a mixture of amorphous material and nanocrystalline regions, with Raman peaks ranging between 490 and 510 cm^{-1} (the zone center phonon for crystalline Si lies at 521 cm^{-1}). (b) Samples containing large amounts of nanocrystalline material and/or O (N) impurities exhibited a strong luminescence background in the 1500–4200 cm^{-1} ($\lambda = 557 - 656$ nm) region. The spectra shown here are for different density-separated batches from a single sample prepared from NaSi + NH$_4$Br at 200 °C, that contained significant O, N and H impurities (10–15 at% by bulk analysis), and also showed the presence of nanocrystals. The largest fluorescence is obtained for the fraction with greatest density ($>$2.1 g/cm^3).

weak feature at $2250 \, cm^{-1}$, that can be assigned to O_3SiH species. In the high frequency region (Fig. 5(b)), features at 3630, 3350 and $2935 \, cm^{-1}$ superimposed upon high-order excitations from the a-Si matrix, reveal the presence of O–H and perhaps N–H vibrations within the sample. The data in Fig. 5 show superimposed the spectra from different density fractions separated within the sample (synthesized at $200 \, °C$ from $NaSi + NH_4Br$). The lightest fraction ($< 1.75 \, g/cm^3$) shows the least amount of Si–H impurities (weakest feature at
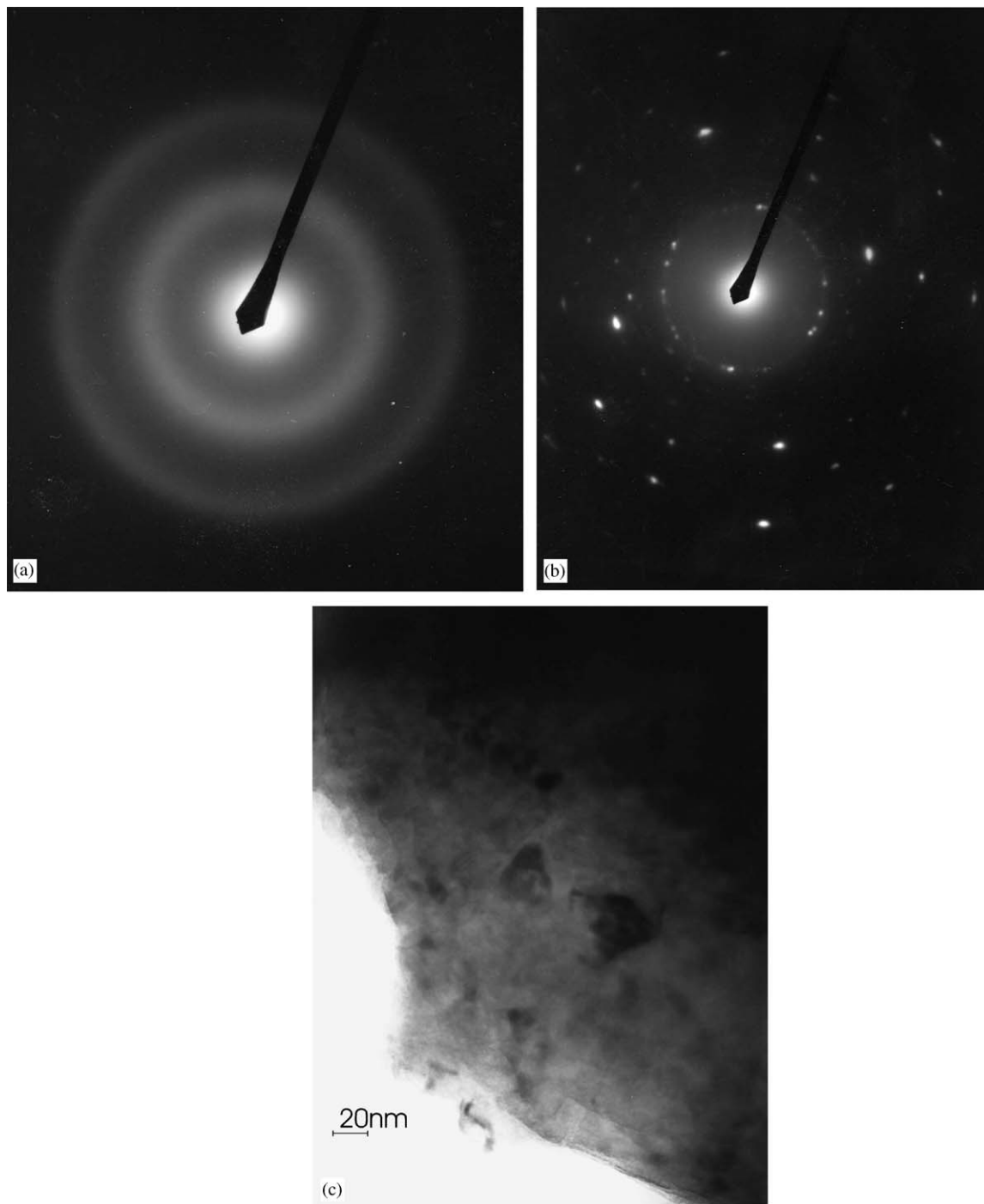

Fig. 9. (a) Selected area microdiffraction patterns in TEM showing the predominantly amorphous nature of the matrix material in samples prepared by reactions (1) and (2). (b) Selected area diffraction pattern showing the presence of crystalline material, within nanocrystalline areas as shown in the TEM image below. The first diffuse ring occurs at $2.52 \, Å$, that corresponds well with the FSDP measured by X-ray diffraction of the amorphous material. (c) TEM image showing the presence of 2–20 nm nanocrystalline regions (exhibiting lattice fringes) within the amorphous Si samples prepared in this study. The SAED patterns were collected from areas approximately 100 nm in diameter. The measured positions of the spots correspond to lattice spacings of diamond-structured Si.

$2080\,cm^{-1}$), but otherwise the spectra are nearly identical. Another difference between the density fractions is in the amount of O impurities, revealed by ^{29}Si NMR spectroscopy discussed below: this difference does not show up well in the FTIR spectra.

3.4. NMR spectroscopy

The highest purity samples of a-Si synthesized in this study (i.e., with minimal or undetectable quanitties of O,N impurities, and with H contents ranging from 5 to 10 at%) exhibited a single broad Gaussian peak in the single pulse ^{29}Si NMR spectrum with its maximum between -60 and $-70\,ppm$ (relative to tetramethyl silane: TMS), and a peak width at half maximum (FWHM) $\sim70\,ppm$ (Fig. 6). The corresponding peak for crystalline Si occurs at $-80\,ppm$, with FWHM = 6 ppm. Previously ^{29}Si MAS NMR spectra have been recorded for a-Si samples prepared by sputtering methods [52]: these samples exhibited an asymmetric NMR peak with FWHM ~70–$80\,ppm$, with its maximum between -40 and $-50\,ppm$. The reason for the difference between the two results is not yet understood. The r.f. sputtered samples certainly exist in a different, probably higher energy, state of structural relaxation than the samples prepared by chemical synthesis at lower temperature, and they likely contain a smaller concentration of Si–H species. It is well known that the ^{29}Si spectra and chemical shifts among Si polymorphs and other Si-containing species are sensitive to small structural variations in the bond length and angle distribution, as well as to the nature of ligands attached to the Si atoms [53]. It is quite likely that differences in the Si–Si bond lengths and SiSiSi angles between the r.f. sputtered samples and our materials prepared by chemical precursor synthesis. It is also possible that a difference in H content between our and the previous samples could influence the NMR spectra. In our study, we also obtained ^{1}H–^{29}Si CP spectra for various a-Si samples: these gave rise to nearly identical spectra to those for the single-pulse ^{29}Si MAS studies (perhaps shifted to slightly less negative ppm values), indicating that the H atoms present within the samples are distributed approximately homogeneously relative to the different Si sites in the amorphous structure (Fig. 6(b)).

Among samples that showed clear presence of O impurities, the NMR spectra usually showed an additional feature that could be correlated with the presence of SiO_x species in the sample (Fig. 7). An "extra" peak was often present at approximately $-104\,ppm$, that lies close to the ^{29}Si NMR peak of amorphous SiO_2 ($-110\,ppm$ [53]). This peak was usually least prominent among samples synthesized at higher temperatures. (Fig. 7(b)), indicating that the lowest T samples were most prone to oxidation during washing and subsequent exposure to air (O_2/H_2O-rich environments). Further,

among samples that were density-separated into fractions, the lowest density fraction exhibited the largest amount of O contamination (Fig. 7(c)).

3.5. Raman and photoluminescence spectra

Most Raman spectra recorded for samples prepared within this study were identical with previous determinations for amorphous silicon, and were dominated by a broad asymmetric Si–Si stretching band with its maximum at $\sim450\,cm^{-1}$ (Fig. 2). However, some samples exhibited Raman features that indicated the formation of nanocrystalline silicon particles within the amorphous matrix [49,55–57]. For example, a sample prepared via reaction (2) at 300 °C showed a sharp Raman peak at $508\,cm^{-1}$, in addition to the broad amorphous feature near $450\,cm^{-1}$ (Fig. 8). The Raman-active phonon mode of bulk crystalline Si occurs at $521\,cm^{-1}$: this is shifted to higher or lower frequency by compressive or tensile stresses acting on crystalline samples, or by surface oxidation; however, the maximum shifts associated with these effects are ~1–$3\,cm^{-1}$ [57–59]. Nanocrystalline Si (and Ge) particles typically have their Raman modes shifted to lower wavenumbers because of the reduction in $q = 0$ selection conditions, and also due to structural relaxation occurring within the finite particles [54–56]. The Raman signal observed here is thus due to the appearance of nanocrystalline Si within the amorphous sample, occurring during the
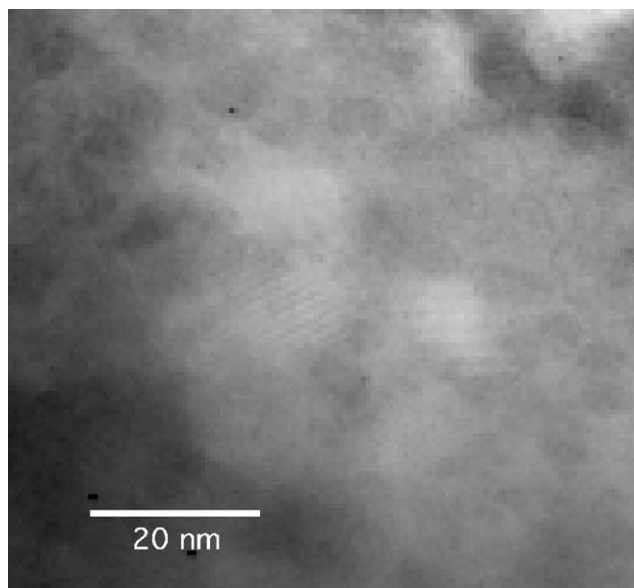

Fig. 10. Enlarged TEM image of a region within one sample of a-Si that contained nanocrystalline material, showing lattice fringes within the nanoparticles. The field of view is approximately 100 nm. The distance between lattice planes is measured to be 2.75 Å, that corresponds to the spacing between Si atoms in a slightly expanded diamond lattice ($a_0 = 5.4301$ Å for $Z = 2$ in the face-centered cubic cell of bulk crystalline material).

solid-state syntheses. The presence of Si nanocrystals was also detected by Raman spectroscopy in samples that had been treated post-synthesis by heating in vacuum in order to reduce the hydrogen content: this procedure is known to induce crystallization in a-Si:H materials [43–46,60,61]. The presence of nanocrystalline particles 2–20 nm across within an amorphous matrix was detected in selected samples studied by TEM and selected area diffraction (Figs. 9 and 10).

During our Raman spectroscopic studies that were originally designed to probe the possible existence of Si–H and/or H–H vibrations, it was noted that some samples exhibited a strong fluorescence background (Fig. 8). Room temperature photoluminescence (PL) spectra were then recorded with the same spectrometer system from 1.35 to 2.4 eV at using 514.5 nm excitation. Different batches of sample exhibited either a strong luminescence with maximum at 1.78 eV (696 nm), or a weaker broad luminescence band maximized at 2.1 eV (590 nm) (Fig. 11).

Further PL measurements were carried out using 476 nm excitation, carefully correcting the spectra for

spectrometer response and temperature effects (black-body) induced by the incident laser. It was found that samples were locally heated during the experiments to approximately 650 K, by absorption of the incident laser. Samples from batches that contained little or no oxygen (or nitrogen) impurities, and that were found to be fully amorphous from Raman and TEM studies, showed no observable PL signal. It is known that only weak PL at ~1.6 eV is obtained from amorphous Si [39].

The strong red luminescence band observed at 1.65–1.78 eV has been associated with the presence of nc-Si particles, that are embedded here within the amorphous matrix [3,4,48,62]: it is thought to arise from quantum confinement excitonic effects within the clusters [2,63]. It is also thought that the PL efficiency may be enhanced by the presence of O and/or N impurities within the matrix, or concentrated at the surface of the nanoclusters [4,6,34,44,48,62,63]. The weaker, broad PL band in the green range (~2 eV) could be associated with oxygen-related defects in the amorphous matrix, such as paramagnetic $\equiv$Si–O$^{\bullet}$ centers [34]. However, discrete Si nanoparticles 1.5–4.0 nm in
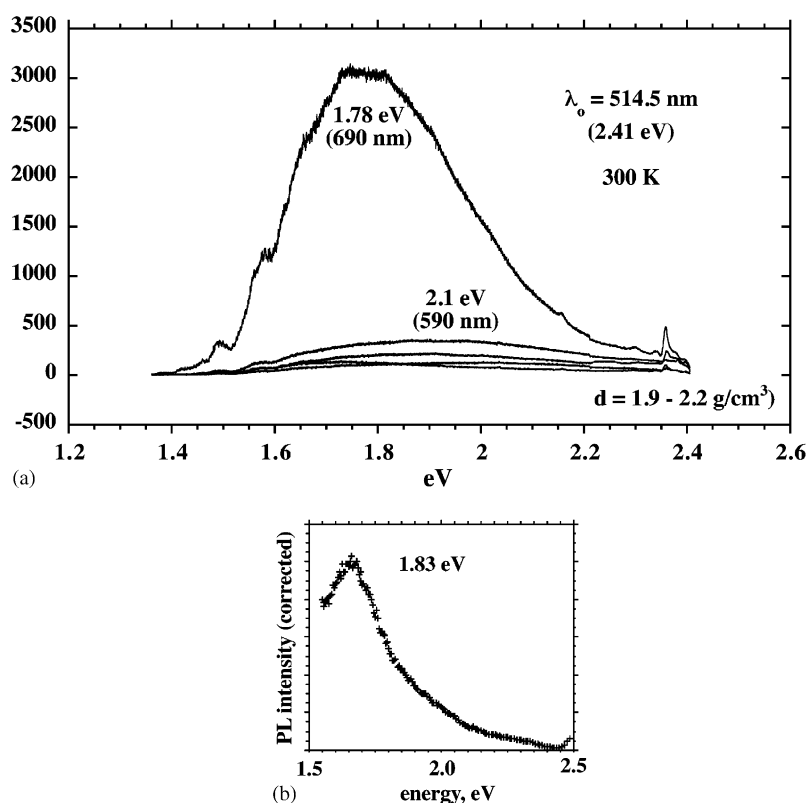

Fig. 11. (a) Room temperature photoluminescence spectra of selected amorphous/nanocrystalline samples of silicon prepared in this study, excited by an Ar^{+} laser ($\lambda = 514.5$ nm; 2.41 eV). The spectra are not corrected for spectrometer response or for thermal excitation effects. The spectra shown here were collected from different density-separated fractions from a single batch of sample, that was shown to contain O, N and H impurities by chemical analysis. The Raman spectra (weak peaks at right) also indicate the presence of nanoparticles. The sample was prepared from NaSi + NH$_4$Cl at 300 °C. Here the strong luminescence at 1.78 eV is observed for the lowest density fraction (<1.75 g/cm^3); fractions with densities 1.9–2.2 g/cm^3 show weaker luminescence at 2.1 eV (cf. spectra in Fig. 8). (b) PL spectrum excited by the $\lambda = 476.5$ nm line of an Ar^{+} laser. The sample is similar to the low-density fraction that gave rise to the strong luminescence at 1.78 eV in the spectra above. The spectrum in (b) has been corrected for spectrometer response and for thermal excitation effects (Planck function: $T = 650$ K) [4,34].

dimension have recently been produced via thermolysis in supercritical hydrocarbon fluids [46,64]. These materials exhibited clear size-dependent PL at 300–320 nm, that is thought to be intrinsic to the unsupported nanoparticles [64]. The origin of the PL in the solid-state samples prepared by metathesis from reactive Zintl phase precursors remains to be determined.

4. Conclusion

We have prepared bulk samples of the amorphous semiconductors Si and Ge using a new solid-state chemical "metathesis" approach, using Zintl phases (e.g., NaSi, NaGe) mixed with metal or ammonium halides as precursors. At sufficiently high synthesis temperatures, depending upon the precursors used and the metathesis procedure followed, the bulk microcrystalline semiconductors were produced. At lower synthesis temperatures, for example in the 200–300 °C range, the materials obtained generally showed only "amorphous" features in their X-ray diffraction patterns. It was later established by Raman scattering and TEM studies that some of these samples in fact contained nanocrystalline semiconductors. Some synthesis runs yielded small amounts of metastable crystalline "semiconductor clathrate" phases, such as Na_8Si_{46}. Some oxidation of the amorphous semiconductor samples occurred during washing steps to remove unwanted products and unreacted starting materials, and also during long-term storage in air. Such oxidation processes could enhance the luminescence efficiency associated with the embedded nanoparticles (red luminescence), and also the intrinsic luminescence associated with broken-bond defects in the amorphous Si/SiO_x matrix. Si nanoparticles were also obtained within the amorphous matrix by annealing to remove hydrogen introduced during synthesis, or were apparently formed directly during the synthesis process, in some cases. All of these parameters could be adjusted by optimizing and controlling the synthesis procedure and post-synthesis treatment steps, to yield a range of amorphous or nano- to micro-crystalline Si and Ge bulk materials, containing variable amounts of O, H and N impurities. These should be further explored for photo- and electro-luminescent or photovoltaic applications.

Acknowledgments

References

[1] A. Shah, P. Torres, R. Tscharner, N. Wyrsch, H. Keppner, Science 285 (1999) 692–698.
[2] L. Brus, J. Phys. Chem. 98 (1994) 3575–3581.
[3] E. Edelberg, S. Bergh, R. Naone, M. Hall, E.S. Aydil, Appl. Phys. Lett. 68 (1996) 1415–1417.
[4] A.J. Kenyon, P.F. Trwoga, C.W. Pitt, G. Rehm, Appl. Phys. Lett. 73 (1998) 523–525.
[5] C.-S. Yang, S.M. Kauzlarich, Y.C. Wang, Chem. Mater. 11 (1999) 3666–3670.
[6] S. Takeoda, M. Fujii, S. Hayashi, Phys. Stat. Sol. (b) 224 (2001) 229–232.
[7] L.H. Lie, M. Duerdin, E.M. Tuite, A. Houlton, B.R. Horrocks, J. Electroanal. Chem. 538–539 (2002) 183–190.
[8] R. Schafer, W. Klemm, Z. Anorg. Allg. Chem. 312 (1961) 214–220.
[9] I.P. Parkin, Chem. Soc. Rev. (1996) 199–207.
[10] I.P. Parkin, Trans. Met. Chem. 27 (2002) 569–573.
[11] R.A. Bley, S.M. Kauzlarich, J. Am. Chem. Soc. 118 (1996) 12,461–12,462.
[12] B.R. Taylor, S.M. Kauzlarich, H.W.H. Lee, G.R. Delgado, Chem. Mater. 10 (1998) 22–24.
[13] E. Soignard, P.F. McMillan, Defect chemistry in γ-Si_3N_4 and γ-Ge_3N_4 spinel nitride phases probed by Raman scattering in the laser-heated diamond anvil cell, Chem. Mater. 16 (2004) 3533–3542.
[14] C. Cros, M. Pouchard, P. Hagenmüller, J. Solid State Chem. 2 (1970) 570–581.
[15] G.K. Ramachandran, J. Dong, J. Diefenbacher, J. Gryko, R.F. Marzke, O.F. Sankey, P.F. McMillan, J. Solid State Chem. 145 (1999) 716–730.
[16] E. Reny, P. Gravereau, C. Cros, M. Pouchard, J. Mater. Chem. 8 (1998) 2839–2844.
[17] D.L. Price, S.C. Moss, R. Reijers, M.-L. Saboungi, S. Susman, J. Phys. C: Solid State Phys. 21 (1988) L1069–L1072.
[18] J.S. Custer, M.O. Thompson, D.C. Jacobson, J.M. Poate, S. Roorda, W.C. Sinke, F. Spaepen, Appl. Phys. Lett. 64 (1994) 437–439.
[19] L.I. Aptekar, Sov. Phys. Dokl. 24 (1979) 993–995.
[20] O. Shimomura, S. Minomura, N. Sakai, K. Asaumi, K. Tamura, J. Fukushima, H. Endo, Philos. Mag. 29 (1974) 547–558.
[21] E. Rapoport, J. Chem. Phys. 46 (1967) 2891–2894.
[22] E.G. Ponyatovsky, O.I. Barkalov, Mater. Sci. Rep. 8 (1992) 147–191.
[23] S.K. Deb, M.C. Wilding, M. Somayazulu, P.F. McMillan, Nature 414 (2001) 528–530.
[24] S. Sastry, C.A. Angell, Nat. Mater. 2 (2003) 739–743.
[25] N. Jakse, L. Hennet, D.L. Price, S. Krishnan, T. Key, E. Artacho, B. Glorieux, A. Pasturel, M.-L. Saboungi, Appl. Phys. Lett. 83 (2003) 4733–4736.
[26] P.F. McMillan, J. Mater. Chem. 14 (2004) 1506–1512.
[27] E. Principi, A.D. Di Cicco, F. Decremps, A. Polian, S. De Panfilis, A. Filipponi, Phys. Rev. B 69 (2004) 201201(4).
[28] M. Wilson, P.F. McMillan, Phys. Rev. Lett. 90 (2003) 135,703–135,707.
[29] P.F. McMillan, Nat. Mater. 1 (2002) 19–25.
[30] J.L. Finney, D.T. Bowron, A.K. Soper, T. Loerting, E. Mayer, A. Hallbrucker, Phys. Rev. Lett. 89 (2002) 205,503–205,507.
[31] C.A. Tulk, C.J. Benmore, J. Urquidi, D.D. Klug, J. Neuefeind, B. Tomberli, P.A. Egelstaff, Science 297 (2002) 1320–1324.
[32] O. Mishima, L.D. Calvert, E. Whalley, Nature 314 (1985) 76–78.

[33] O. Mishima, H.E. Stanley, Nature 396 (1998) 329–335.

[34] A.J. Kenyon, P.F. Trwoga, C.W. Pitt, J. Appl. Phys. 79 (1996) 9291–9300.

[35] N.-M. Park, C.-J. Choi, T.-Y. Seong, S.-J. Park, Phys. Rev. Lett. 86 (2001) 1355–1357.

[36] The ILL experiment resulted from ideas developed between C.A. Angell and H. Schöber regarding the likely low frequency ("boson peak") characteristics of an "ideal glass" such as a-Si, within a collaborative programme developed with A. Toelle and M. Koza. J. Gryko and PFM provided a-Si samples for the study, and assisted with the neutron experiments.

[37] The high H contents in our a-Si samples were determined using ILL instrument D7, developed and directed by Dr. R. Stewart, that permits spin-polarised neutron scattering spectroscopy of materials, to independently examine coherent- and incoherently scattered channels.

[38] Y.J. Chabal, C.K.N. Patel, Phys. Rev. Lett. 53 (1984) 210–213.

[39] Y.J. Chabal, C.K.N. Patel, Phys. Rev. Lett. 53 (1984) 1771–1774.

[40] C.A. Guy, A.C. Wright, R.N. Sinclair, R.J. Stewart, F. Jansen, J. Non-Cryst. Solids 196 (1996) 260–266.

[41] M. Vergnat, S. Houssaïni, G. Marchal, Ph. Mangin, Phys. Rev. B 47 (1993) 7584–7587.

[42] N.H. Nickel, W.B. Jackson, Phys. Rev. B 51 (1995) 4872–4881.

[43] I. Kaiser, N.H. Nickel, W. Fuhs, W. Pilz, Phys. Rev. B 58 (1998) R1718–R1721.

[44] A. Fontcuberta i Morral, J. Bertomeu, P. Roca i Cabarrocas, Mater. Sci. Eng. B 69–70 (2000) 559–563.

[45] M. Katiyar, J.R. Abelson, Mater. Sci. Eng. A 304–306 (2001) 349–352.

[46] L.A. Pell, A.D. Schricker, F.V. Mikulec, B.A. Korgel, Langmuir 20 (2004) 6546–6548.

[47] G. Lucovsky, R.J. Nemanich, J.C. Knights, Phys. Rev. B 19 (1979) 2064–2073.

[48] E. Edelberg, S. Bergh, R. Naone, M. Hall, E.S. Aydil, J. Appl. Phys. 81 (1997) 2410–2417.

[49] D.C. Marra, E.A. Edelberg, R.L. Naone, E.S. Aydil, J. Vac. Sci. Technol. A 16 (1998) 3199–3210.

[50] A. Grzechnik, H.D. Zimmerman, R. Hervig, P. King, P.F. McMillan, Contrib. Mineral. Petrol. 125 (1996) 311–318.

[51] G. Moore, P.F. McMillan, A. Chizmeshya, Geochim. Cosmochim. Acta 64 (2000) 3571–3579.

[52] W.-L. Shao, J. Shinar, B.C. Gerstein, F. Li, J.S. Lannin, Phys. Rev. B 41 (1990) 9491–9494.

[53] G. Engelhardt, D. Michel, High-Resolution Solid-State NMR of Silicates and Zeolites, Wiley, New York, 1987.

[54] A.V. Andrianov, G. Polisski, J. Morgan, F. Koch, J. Lumin. 80 (1999) 193–198.

[55] S.K. Deb, in: M. Yousuf, N. Subramian, K. Govind Rajan (Eds.), Adv. High Pressure Sci. Technol. Proceedings of the IV NCHST, IGCAR, Kalpakkam, India, 1997, pp. 147–152.

[56] A.V. Kolobov, J. Mater. Sci. 12 (2004) 195–203.

[57] Th. Englert, G. Abstreiter, J. Pontcharra, Solid State Electron. 23 (1980) 31–33.

[58] E. Anastassakis, A. Pinczuk, E. Burstein, F.H. Pollak, M. Cardona, Solid State Commun. 8 (1970) 133–138.

[59] J.T. Fitch, C.H. Bjorkman, G. Lucovsky, F.H. Pollak, X. Yin, J. Vac. Sci. Technol. B 7 (1989) 775–781.

[60] J.J. Boland, G.N. Parsons, Science 256 (1992) 1304–1306.

[61] P. Roca i Cabarrocas, J. Non-Cryst. Solids 266–269 (2000) 31–37.

[62] E. Edelberg, S. Bergh, R. Naone, M. Hall, E.S. Aydil, Appl. Phys. Lett. 68 (1996) 1415–1417.

[63] M.J. Sailor, E.J. Lee, Adv. Mater. 9 (1997) 783–793.

[64] J.D. Holmes, K.J. Ziegler, R.C. Doty, L.E. Pell, K.P. Johnston, B.A. Korgel, J. Am. Chem. Soc. 123 (2001) 3743–3748.